Article

Finite Element-Based Simulation for Edgewise Compression Behavior of Corrugated Paperboard for Packaging of Agricultural Products

Jongmin Park [1], Minjung Park [2], Dong Soo Choi [3,*], Hyun Mo Jung [4,*]
and Sung Wook Hwang [5]

[1] Department of Bio-Industrial Machinery Engineering, Pusan National University, Miryang 50463, Korea; parkjssy@pusan.ac.kr
[2] Department of Agricultural Engineering, National Institute of Agricultural Sciences, Rural Development Administration, Wanju 55365, Korea; mjpark0107@korea.kr
[3] Postharvest Engineering Division, National Institute of Agricultural Sciences, Rural Development Administration, Wanju 55365, Korea
[4] Department of Logistic Packaging, Kyoungbuk Science College, Chilgok 39913, Korea
[5] Department of Chemical Engineering, Keimyung University, Daegu 42601, Korea; swhwang@kmu.ac.kr
* Correspondence: choi0ds@korea.kr (D.S.C.); hmjung@kbsc.ac.kr (H.M.J.)

check for updates

Abstract: Since most goods are transported and stored in a unit-load form in today's global supply chain, there has been a growing concern regarding the compression strength of corrugated paperboard boxes for packaging of agricultural products. The best predictor of the compression strength of corrugated boxes is the edgewise compression test (ECT) value; therefore, its efficient measurement or prediction is crucial for the design of more efficient corrugated boxes for food and agricultural and industrial products. This study investigated the edgewise compression behavior (load vs. displacement plot, ECT, and failure mechanism) of corrugated paperboard based on different types of testing standards and flute types using finite element analysis (FEA) and experimental analysis. The results of this study showed that the magnitude of the ECT values produced by the FEA was different from the values produced by the experiment. The difference in the ECT can be possibly explained by layer thickness approximations, together with glue line width assumptions between fluting and the liners in the numerical models. However, the trends of the values were the same. If the material properties of corrugated paperboard components and modeling methods of the corrugated paperboard are further studied, the FE (finite element)-based simulation technique will be a useful alternative tool that can replace the edgewise compression test.

Keywords: corrugated paperboard; edgewise compression test; finite element analysis; computer simulation; failure mechanism; mechanical test

1. Introduction

A large amount of corrugated paperboard is used for packaging (primarily for box construction to protect and transport goods) due to its high strength-to-weight ratio, recyclability, and biodegradability [1,2].

Many factors affect the overall strength and performance of the corrugated paperboard and corrugated paperboard box including mechanical properties of the components (liner, corrugating medium, and adhesive), manufacturing quality, machine precision, and human factors involved in the corrugation process [3].

Paper is an orthotropic material having different mechanical properties for each of the three principal material orientations [4]: Out-of-plane (thickness) direction (*z*), in-plane direction parallel to the rolling during processing (machine direction (MD)), and the in-plane direction normal to MD (cross direction (CD)), due to it having a different manufacturing process. Paper also has a highly non-linear behavior and large differences between tensile and compressive stiffness and strength for both MD and CD that limits the application of simple material models during numerical or finite element (FE) modeling [5].

The manufacturing direction (wave propagation) of the corrugated paperboard coincides with the MD of the liners. The flute direction and the out-of-plane (thickness) direction of the corrugated paperboard coincide with the CD and *z*-direction of the liners, respectively (Figure 1). Therefore, the corrugated paperboard is an orthotropic sandwich structure, which has liners providing bending stiffness and flutes providing shear stiffness [6,7].
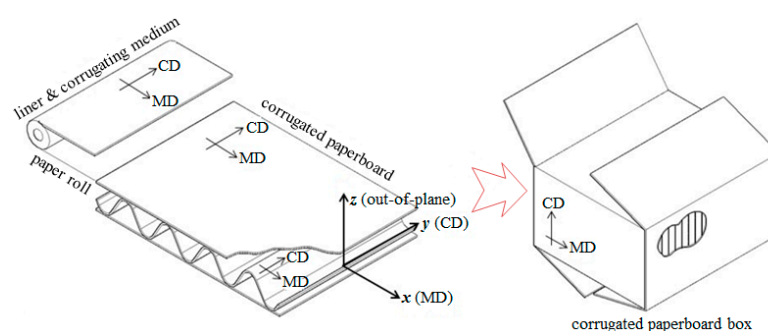

Figure 1. Orthotropic properties of corrugated board components (fiber orientation) and corrugated paperboard (flute direction).

When top-to-bottom compression force is applied to a corrugated paperboard box, the four vertical edges and the side panels of the box support the compression force. Under compression force, the vertical edges of the box experience edgewise compression along the CD, and the side panels of the box experience bending along both the CD and MD. Therefore, the box compression test (BCT) value can be determined by both the edgewise compression test (ECT) value for CD and bending stiffness for CD and MD [6,8–10].

The ECT value of the corrugated paperboard is used as a primary indicator representing the quality and compression strength of the corrugated paperboard box [11]. The shape and dimensions of the ECT specimens are different depending on various testing standards. There are four ECT methods used based on the various restrictions of the edge failure and bending behavior of the test specimen: (a) Edge-clamping method [12,13], (b) neck-down method [13,14], (c) rectangular test specimen method with small slenderness ratio [13,15–17], and (d) edge-reinforced method (wax coating) [18–20]. Figure 2 shows a representative test specimen for each of the four methods.

Markström [21] found that the ECT value of the corrugated paperboard was the highest for the TAPPI T 838, followed by TAPPI T 811 and FEFCO No.8. The difference in the ECT value was the smallest (approximately 15 kN/m) between the neck-down method in TAPPI T 838 and the edge-reinforcement method in TAPPI T 811, and was an average of 31% between TAPPI T 838 and FEFCO No.8. The study pointed out that there was difficulty in defining the inherent characteristic value of particular corrugated paperboard due to the large difference in the ECT value, which was a result of the different test standards. The study concluded that the best method to describe the behavior of the corrugated paperboard under pure compression was the neck-down method in TAPPI T 838.

Popil [11] compared the ECT value between TAPPI T 811, 838, and 839 for a single-wall (SW) corrugated paperboard. The study found that there is no clear trend in the difference of the ECT values between these standards as a function of the basis weight of the corrugating medium. The ECT value measured by T 839 was much less than the ECT measured by other standards when the basis weight of

the corrugating medium was small. However, it was much higher than the ECT measured by others when the basis weight of the corrugating medium was large. The study concluded that the clamping pressure and out-of-plane flat crush resistance in T 839 affected the results.
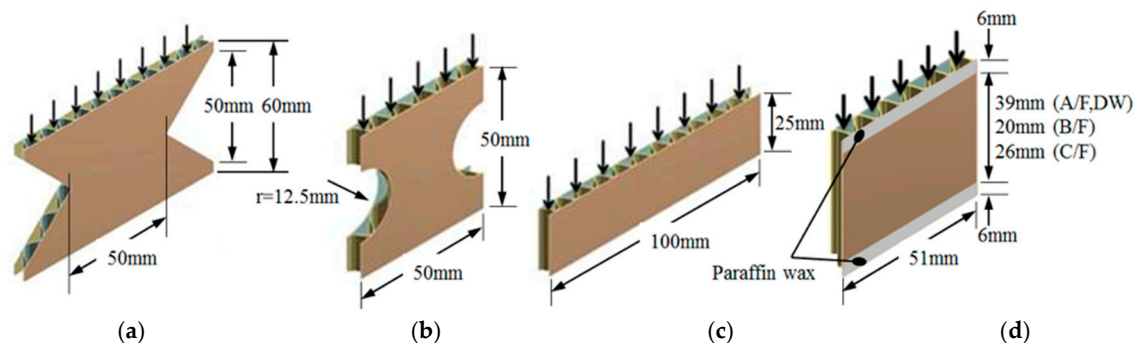

Figure 2. Various test specimens for measuring the edgewise compression test (ECT) value of corrugated paperboard; they should be listed as: (**a**) KS M 7063-1 method A; (**b**) TAPPI T 838; (**c**) FEFCO No.8; (**d**) ISO 13821.

The conditions to produce an acceptable ECT value can be summarized into four points: (a) Measure what is intended to measure, i.e., pure compression strength of the whole corrugated test specimen, (b) accurate and (c) reproducible, and (d) easy to perform as a routine method in a corrugated paperboard laboratory [6,21].

Experimental methods for investigating the performance and properties of the corrugated paperboard and corrugated paperboard-based products have limitations from time and economic perspectives. In addition, it is impossible to quantitatively analyze the effect of each component of the corrugated paperboard on ECT. Therefore, computer simulation techniques like finite element analysis (FEA) recently have been used to analyze various characteristics including ECT of corrugated paperboard [1–3,7,10,22,23].

Most FEA studies have focused on analyzing mechanisms of buckling, failure, stability, and adherence strength of corrugated paperboard [1–3,24,25] and investigating compression and flexural behavior of different flute types [10]. Some FEA studies have also tried to optimize board combinations of corrugated paperboard, to analyze performance and strength of corrugated paperboard boxes, and to develop FEA simulations to replace the conventional semi-empirical equations [22,26,27].

Since paper has a complex mechanical behavior representing orthotropic material properties and high non-linearity, specific material models and advanced FE techniques have been required for analyzing paper-based products like the corrugated paperboard. Therefore, some researchers [7,23,24,28] conducted studies to investigate equivalent stiffness properties to develop simplified FE models for corrugated paperboard.

Jiménez and Liarte [22] conducted FEA for ECT specimens cut based on the recommendations of FEFCO No.8 testing standard. They found that frictional contact conditions between the modeled test specimen and the rigid surface did not significantly affect the ECT value for A/F (A-flute) and C/F (C-flute) (difference due to the frictional contact condition was less than 3%). However, there was an approximately 15% difference in B/F depending on the frictional contact condition.

Gospodinov et al. [29] analyzed the effect of the Young's modulus of its components on the overall Young's modulus of C/F corrugated paperboard using an analytical method. They found that liners affected much more mechanical strength of the corrugated paperboard than corrugating mediums since the gradient of Young's modulus between the liners and corrugated paperboard was approximately 88 times higher than the gradient of the Young's modulus between the corrugating medium and corrugated paperboard.

The FEA has been successfully used to predict the mechanical properties of the corrugated paperboard; however, a study analyzing the various test methods of ECT is rare. This study analyzed

the edgewise compression behaviors for single-wall (A/F and B/F) and double-wall (AB/F and BB/F) corrugated paperboard that are commonly used in South Korea [30] with three standardized methods (KS M 7063-1 method A, TAPPI T 838, and FEFCO No.8), using FE-based simulation and experimental methods.

2. Materials and Methods

2.1. Edgewise Compression Test

The edgewise compression test (ECT) values of two single-wall (A/F and B/F) and two double-wall (AB/F and BB/F) corrugated paperboards that are used in packaging of agricultural products were measured using the guidelines of KS M 7063-1 method A [13], TAPPI T 838 [14], and FEFCO No.8 [15] testing standards. Inaccurate cutting of the test specimen led to decreased mechanical strength up to 14% [31]. To prevent mechanical strength loss due to inaccurate cutting of the test specimen, a customized rotary blade-type sample-cutting machine was used in this study (Figure 3). The cutting machine also had a sample holder to make a circular neck-down section that was required in TAPPI T 838.
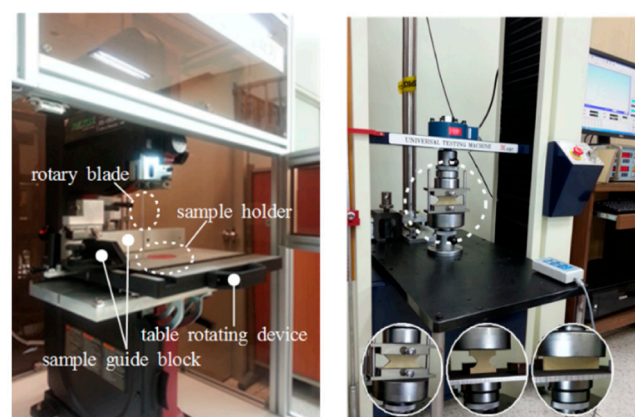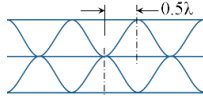

Figure 3. Rotary blade type sample cutting machine and the experimental setup for measuring the ECT values.

The fabricated test specimens were pre-conditioned at 23 °C and 50% relative humidity for at least 72 h before testing. The ECT was conducted following testing conditions and procedures of each testing standard using a universal testing machine (KST in South Korea, 980 N) (Figure 3). For TAPPI T 838 and FEFCO No.8, sand paper was attached to the vertical loading plate to prevent sliding of the test specimen. The testing was performed using five replicates for each standard and flute type.

The board combinations of corrugated paperboard used in this study were SK180/K180(A/F)/SK180 for A/F corrugated paperboard, SK180/K180(B/F)/SK180 for B/F corrugated paperboard, SK180/K180(A/F)/ K180/K180(B/F)/SK180 for AB/F corrugated paperboard, and SK180/K180(B/F)/K180 /K180(B/F)/SK180 for BB/F corrugated paperboard, where K180 was made of 100% Korean old corrugated container (KOCC) and SK180 was made of 20% unbleached kraft pulp (UKP) + 80% KOCC. The measured specifications of these corrugated paperboard are shown in Table 1.

Table 1. The measured specifications of the corrugated paperboards used in the study.

Components		Thickness (mm)	Wavelength (λ) (mm)	Height of Flute (h) (mm)	Take-Up Factor	Flutes per 300 mm Liner
Flute	A/F	0.22	9.00 (8.33~9.38)	4.90 (4.5~4.8)	1.560 (1.6)	33 (34 ± 2)
	B/F	0.22	6.00 (5.27~6.25)	2.65 (2.5~2.8)	1.424 (1.4)	50 (50 ± 2)
Liner	Inner & outer	0.20				
	Middle	0.22		BB/F-DW:		

Notes: KS T 1034 [32].

2.2. FE Modeling and Analysis Procedures

The finite element (FE) model was created based on the physical specifications (Table 1) of the two single-wall (A/F and B/F) and two double-wall (AB/F and BB/F) corrugated paperboards used during the ECT test. The geometrical shape of the flute was modeled as a cosine function. According to Armentani et al. [7], the phase angle between two flutes (having the same flute type) did not significantly affect the buckling strength during edgewise compression using the double-wall corrugated paperboard. Therefore, the FE model for the test specimens made of BB/F was built by aligning the flute tops and flute bottoms with a phase shift of 0.5λ and 180° (Table 1). The connection point between the liner and flute of the corrugated paperboard was modeled using a sharing method for the point (nodes) for simplification. The allowable gap between surfaces was given by assigning pinball regions to raise the convergence in the case of large deformations. The shape of the specimen was defined in KS M 7063-1 method A [13], TAPPI T 838 [14], and FEFCO No.8 standards [15], respectively.

The FE model used SOLID187 element for KS M 7063-1 method A and TAPPI T 838; SOLID186 element for FEFCO No.8 [33]. The models were meshed to produce 21,800 (A/F)~53,916 (BB/F) finite elements for KS M7063-1 method A, 10,064 (A/F)~24,027 (BB/F) finite elements for TAPPI T 838, and 5356 (B/F)~13,020 (AB/F) finite elements for FEFCO No.8, while the total number of nodes was 44,993 (A/F)~104,256 (BB/F) for KS M7063-1 method A, 21,242 (A/F)~47,202 (BB/F) for TAPPI T 838, and 38,838 (B/F)~85,356 (BB/F) for FEFCO No.8. Figures 4 and 5 show examples of the meshed FE models for A/F and AB/F corrugated paperboard prepared following the requirements of each standard.
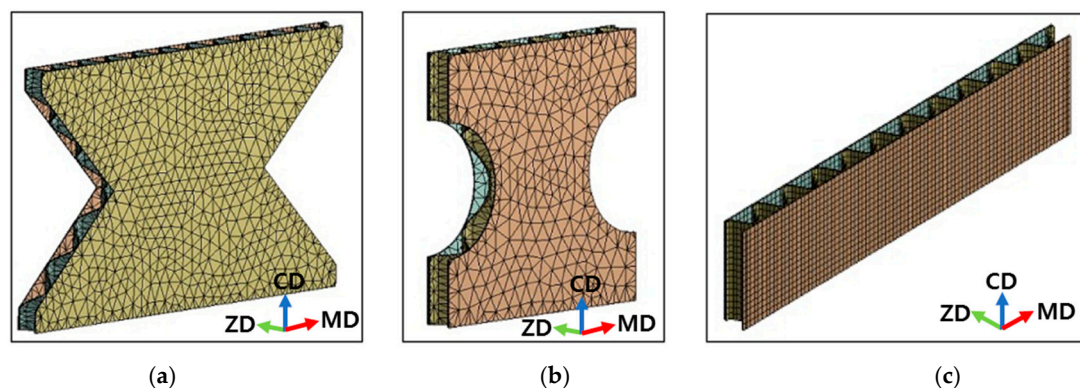

(**a**)　　　　　　　　　　(**b**)　　　　　　　　　　(**c**)

Figure 4. The meshed 3D models for FE simulation of A/F corrugated paperboard; they should be listed as: (**a**) KS M 7063-1 method A; (**b**) TAPPI T 838; (**c**) FEFCO No.8.
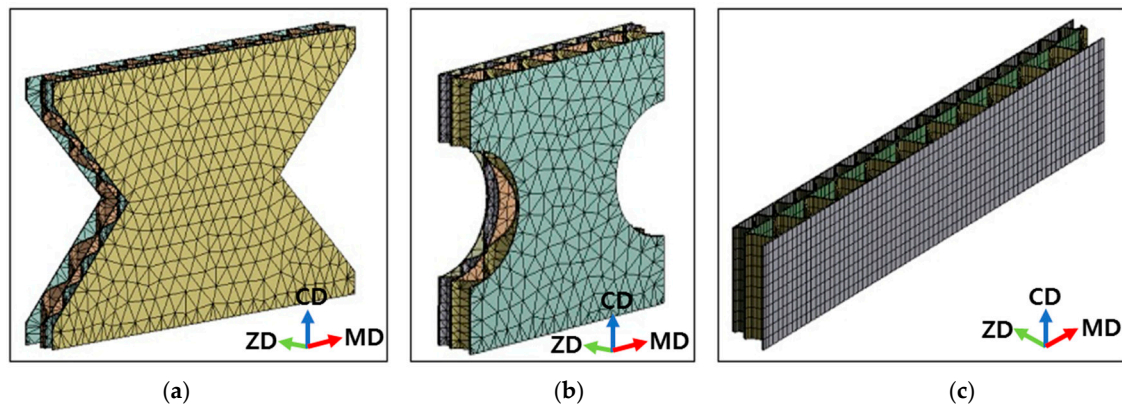
Figure 5. The meshed 3D models for finite element (FE) simulation of AB/F (A/F + B/F) corrugated paperboard; they should be listed as: (**a**) KS M 7063-1 method A; (**b**) TAPPI T 838; (**c**) FEFCO No. 8.

Before selecting the mesh size, the mesh convergence study was conducted to reassure that the employed mesh element size is neither time consuming nor leading to any discretization error. In this simulation, the mesh study includes five different element mesh sizes. Table 2 shows von Mises stress of different mesh size of A/F by KS M 7063-1 method A using FEA. It can be seen from Table 2 that stress is similar for the mesh size ranging from 1.3 to 1.7 mm. By considering the least number of distorted elements and the time taken to run the simulation, mesh size of 1.3 mm was chosen for the remaining study.

Table 2. von Mises stress of different mesh size of A-flute (A/F) by KS M 7063-1 method A using finite element analysis (FEA).

Mesh Size (mm)	von Mises Stress (MPa)
1.3	20.3
1.4	20.9
1.5	19.8
1.6	19.2
1.7	18.3

The post-processor used for the study was ANSYS® FE [33]. Nonlinear/large displacement conditions were applied to the analysis due to the material properties of the corrugated paperboard. For the KS M 7063-1 method A, translation and rotation motions of both ends of the modeled test specimen were constrained against the x, y, and z-axis in the simulation [34] because 20 mm of test specimens' top and bottom was secured by clamps in the experimental set-up of KS M 7063-1 method A.

For TAPPI T 838 and FEFCO No.8, a pinned connection was defined for the ends of the modeled test specimen [34]. This was because the bearing power did not affect the buckling behavior of the test specimen, although the lower section of the test specimen was supported by metal guide blocks until a 50 N load was applied to the test specimen in the actual experiment. The frictional contact condition was applied to locations (left and right portions of the sharing points between the liner and flute of the corrugated paperboard) where the liners and flutes were expected to be contacted during the edgewise compression.

To apply the load to the specimen, the upper surface of the modeled test specimen was displaced downward with 12.5 mm/min speed simulating the deformation caused by moving plates of a compression tester [13–15]. The reaction force applied to the lower surface of the test specimen was analyzed to complete the load vs. displacement plots.

2.3. Material Properties

The required material properties for FEA were Young's modulus, Poisson's ratio, shear modulus, yield strength, and frictional coefficient between the corrugated paperboard components. The corrugated paperboard components such as liners and corrugated mediums were assumed to be orthotropic materials, which means their material properties have symmetry for x(MD), y(CD), and z-plane (Figure 1). Therefore, each board had nine elastic material properties, such as E_x, E_y, E_z, G_{xy}, G_{xz}, G_{yz}, μ_{xy}, μ_{xz}, μ_{yz}, and two strength values, $\sigma_{y\text{-MD}}$ and $\sigma_{y\text{-CD}}$ [34].

Among the material properties described above, the E_x and E_y, in-plane Elastic moduli, and the $\sigma_{y\text{-MD}}$ and $\sigma_{y\text{-CD}}$ values were calculated using the load vs. elongation plots (Figure 6) of an uniaxial tensile test (tensile tester: KST, capacity: 100 kgf, extensometer resolution: 0.01 mm, max. tensile force of pneumatic grip: 2 kN) based on ISO 1924 [35].
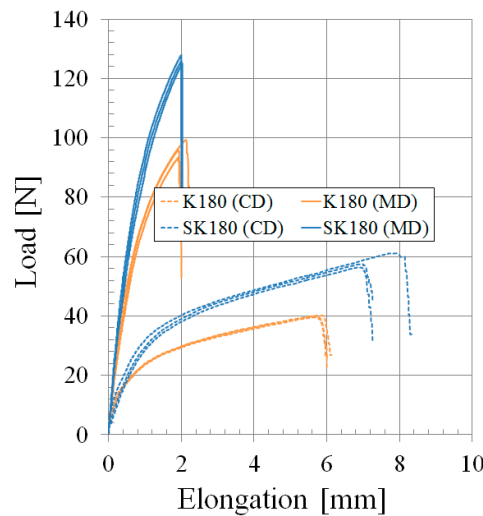

Figure 6. Load vs. elongation plots for the corrugated paperboard components. (CD—cross direction, MD—machine direction).

Based on the shape of the load vs. elongation plot, the stress–strain behavior of the liner and medium was assumed to be linear elastic to simplify the model. Due to the difficulty of measuring the other material properties as a result of the thickness of the paper, these material properties are typically estimated.

The Poisson ratio of the material was obtained from Nordstrand [28], E_z out-of-plane elastic modulus was estimated using Equation (1) [36], and shear modulus was estimated using Equation (2) [4,37]. The final material properties used for the FE model are presented in Table 3.

$$E_z = E_x/200 \tag{1}$$

$$G_{xy} = 0.387\sqrt{E_x E_y},\ G_{xz} = E_x/55, G_{yz} = E_y/35 \tag{2}$$

Table 3. Orthotropic material properties of corrugated paperboard components used for the FEA.

Paperboards	Young's Modulus (GPa)			Poisson's Ratio [1]			Shear Modulus (GPa)			Yield Strength (MPa)	
	$E_x(E_{MD})$	$E_y(E_{CD})$	E_z	μ_{xy}	μ_{xz}	μ_{yz}	G_{xy}	G_{xz}	G_{yz}	$\sigma_{y\text{-MD}}$	$\sigma_{y\text{-CD}}$
K180	2.20 (±0.02)	0.37 (±0.01)	0.011	0.34	0.01	0.01	0.349	0.040	0.010	29.09 (±0.8)	12.12 (±0.1)
SK180	3.16 (±0.07)	0.40 (±0.01)	0.016	0.34	0.01	0.01	0.435	0.057	0.011	42.50 (±0.8)	19.50 (±0.5)

Notes: The values in parentheses are standard deviation values. [1] Nordstrand [28].

As the flute deformation in edgewise compression proceeded, the contact area between the flute and liner on the left and right portions of the shared nodes increased gradually. Accordingly, the frictional contact conditions at a portion where contact was expected were used to accurately analyze the edgewise compression behavior of corrugated paperboard. The static-frictional coefficients for various contact conditions between corrugated paperboard components were measured based on ISO 15359 [38] using a frictional test device reported by Park et al. [39]. Figure 7 shows the static-frictional coefficient used for the model.
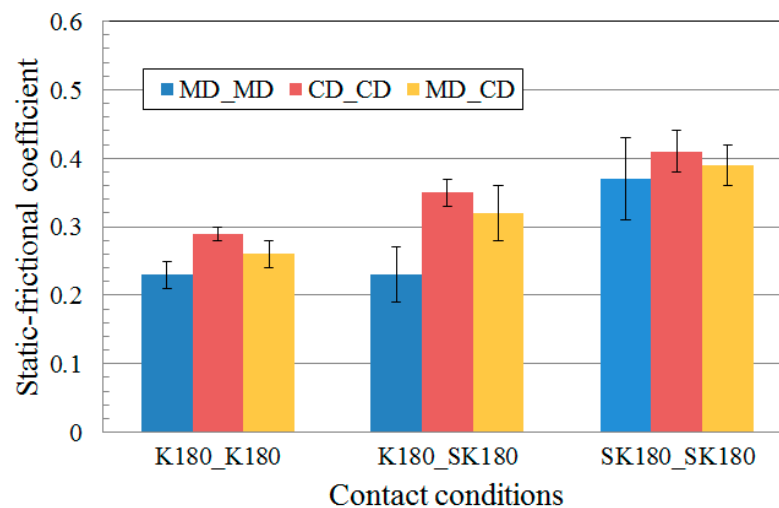

Figure 7. Static-frictional coefficients between corrugated paperboard components.

3. Results and Discussion

3.1. FE Simulation for Edgewise Compression Behavior

Figure 8 shows the load vs. displacement plots predicted using the FE model by flute types and standards. For all standards, the double-wall (DW) and single-wall (SW) corrugated paperboard had significantly different gradient and peak points of the load-deflection plots. For the FE model built based on the KS M 7063-1 method A [13], which is an edge clamping method, the peak points of AB/F and A/F were greater than those of BB/F and B/F, respectively. However, for the models built based on the FEFCO No.8 method [15], which is a rectangular test specimen method with a small slenderness ratio, there was an opposite trend compared to the KS M 7063-1. The trend change was the consequence of the relatively small slenderness ratio of the FEFCO No.8 test specimen (Table A2 in Appendix A), resulting in a reduced effect of the corrugated paperboard thickness on the edgewise compression behavior.

Both SW and DW corrugated paperboard had similar gradients in the elastic region. The stiffness of the DW corrugated paperboard was higher than the stiffness of the SW corrugated paperboard.

The failure mechanism for each test method and flute type was analyzed using the distribution of stresses and deformation at the peak point of the load vs. displacement plot (Figures 9 and 10).

For the KS M 7063-1 method A and the TAPPI T 838 FE models, where test specimens were neck-down at the middle, local buckling of the liners around the neck-down section was observed. In particular, the stress concentration was observed close to the edge of the neck-down section. For the FEFCO No.8 FE models, the stress was distributed evenly to the entire surface, and therefore local buckling of the liners was uniformly observed over the entire surface of the specimen. The stress distribution and the local buckling shape for the rectangular test specimen of the FEFCO No.8 was similar to the results observed by Haj-Ali [2] for different rectangular test specimens (5.08 × 5.08 cm (TAPPI T 839) and 3.81 × 5.08 cm (non-standard ECT geometry)).

Unlike A/F, B/F, and BB/F, whose neutral axis was placed at the middle of the corrugated paperboard thickness (*z*-direction) (Table A1 in the Appendix A), AB/F had bulging toward the B/F direction due to the higher compression stress generated at the inner liner connecting the A/F to the B/F. Once bulging had occurred, the inner liner became a compression state and the outer liner became a tension state. The bulging of AB/F was shown for TAPPI T 839; however, it was not observed for the FEFCO No.8 specimens due to their small slenderness ratio.
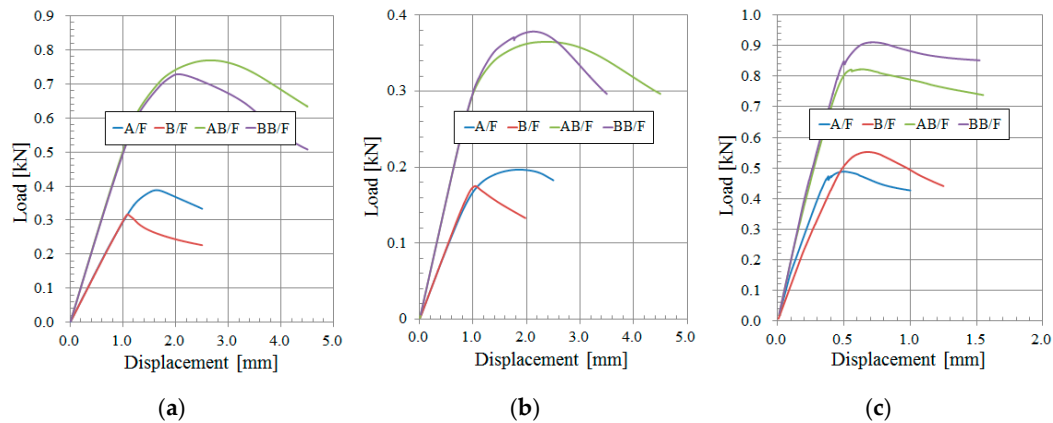

Figure 8. FE simulation results (load vs. displacement plots) for edgewise compression behavior; they should be listed as: (**a**) KS M 7063-1 method A; (**b**) TAPPI T 838; (**c**) FEFCO No.8.
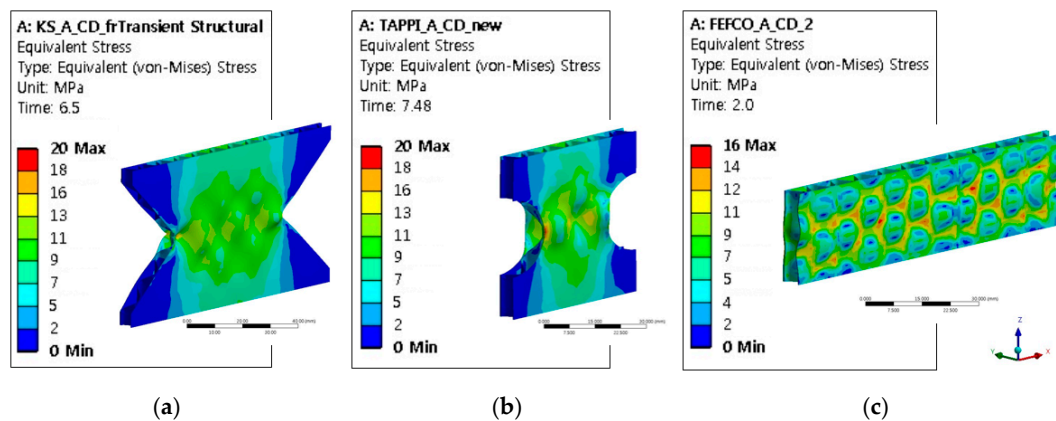

Figure 9. Stress distribution at the peak of the load vs. displacement plot of A/F corrugated paperboard; they should be listed as: (**a**) KS M 7063-1 method A; (**b**) TAPPI T 838; (**c**) FEFCO No.8.
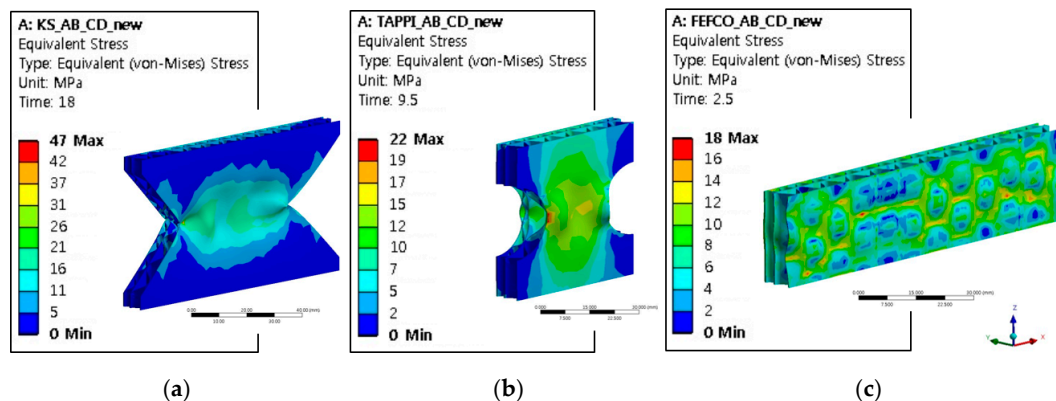

Figure 10. Stress distribution at the peak of the load vs. displacement plot of AB/F corrugated paperboard; they should be listed as: (**a**) KS M 7063-1 method A; (**b**) TAPPI T 838; (**c**) FEFCO No.8.

3.2. Comparison with Experimental Study

Load vs. displacement plots for each standard and flute type (both experimental and FEA results) are shown in Figures 11 and 12, and ECT values analyzed from these plots are shown in Figure 13. The load vs. displacement plot of the experiment showed a lower initial stiffness region (circled area in Figure 11) potentially caused by the initial flattening and crushing of the top and bottom cutting surface. This segment of the plot was missing from the plots produced by the FEA because the FE model assumed perfect samples and could not model damage caused by the sample preparation process.
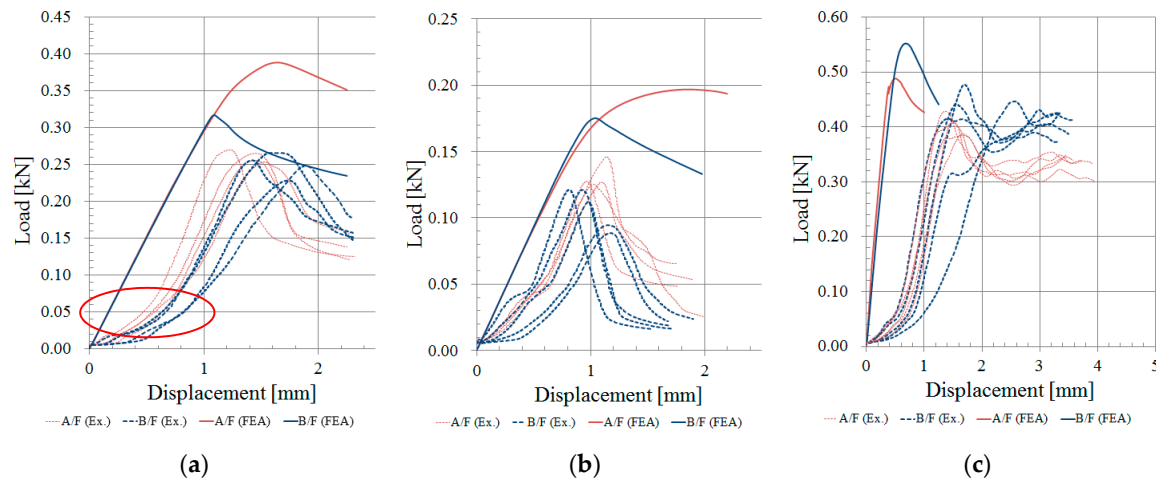

Figure 11. Comparison of load vs. displacement plots produced by the FE model and the experiment for single-wall corrugated boards, they should be listed as: (**a**) KS M 7063-1 method A; (**b**) TAPPI T 838; (**c**) FEFCO No.8.
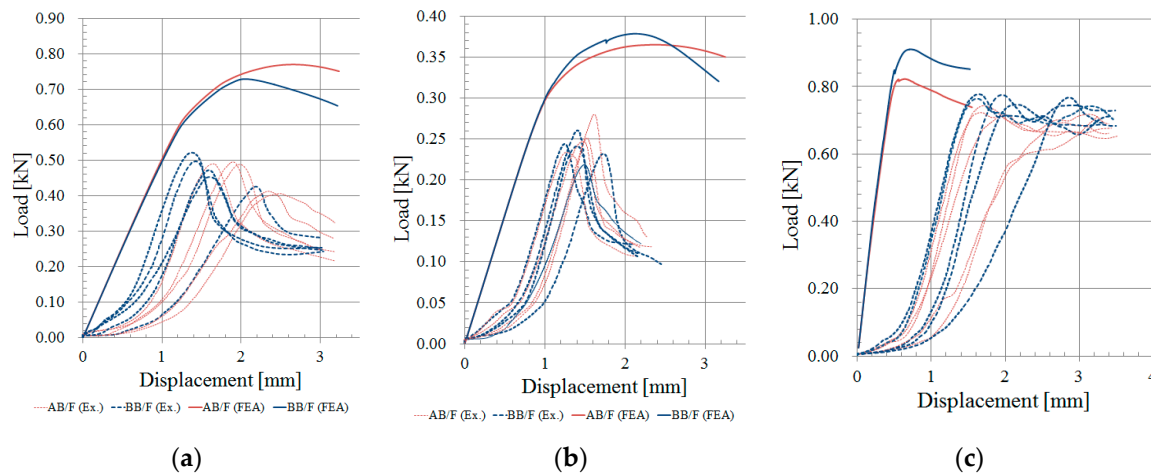

Figure 12. Comparison of load vs. displacement plots produced by the FE model and the experiment for double-wall corrugated boards; they should be listed as: (**a**) KS M 7063-1 method A; (**b**) TAPPI T 838; (**c**) FEFCO No.8.

When the measured ECT values were compared to the FE prediction, it was found that the FE model consistently overpredicted the measured ECT values by approximately 19 kN/m (FEFCO No.8)~43 kN/m (KS M 7063-1 method A). The difference between the measured ECT of KS M 7063-1 method A and TAPPI T 838 was small, but the measured ECT values of FEFCO No.8 were consistently less than that of KS M 7063-1 method A and TAPPI T 838: 33% less (A/F), 19% less (B/F), 27% less (AB/F), and 25% less (BB/F). This agrees with the results found by other studies; in particular, Markström [21] found that there was a 31% ECT difference between TAPPI T 838 and FEFCO No.8. Based on the one-way ANOVA analysis [40] shown in Table 4, there was not a statistically significant difference

between ECT values measured using KS M 7063-1 method A and TAPPI T 838 ($p > 0.05$), but there was a significant difference between ECT values measured using FEFCO No.8 and the other two standards ($p < 0.05$). Similar to the FE prediction for the KS M 7063-1 method, AB/F and A/F had greater ECT than BB/F and B/F, while for FEFCO No.8 the opposite trend was observed. For TAPPI T 838, there was a mixed trend compared to the other standards.
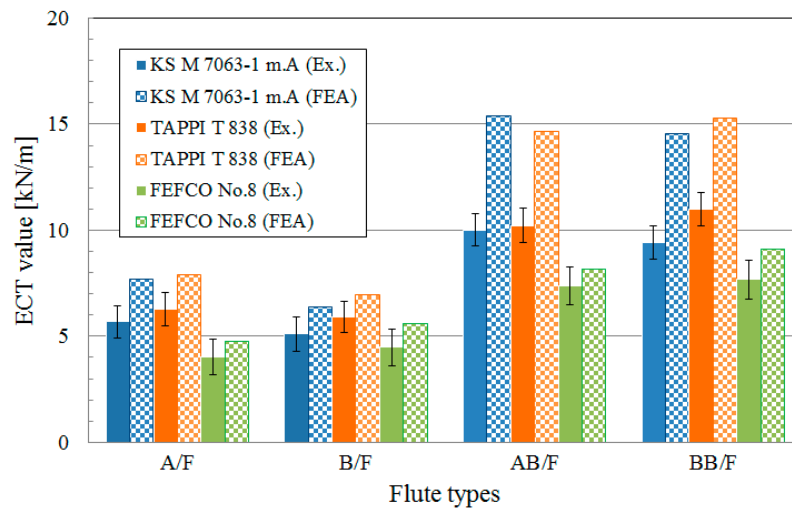

Figure 13. ECT values according to standards and flute types.

Table 4. ECT values and one-way ANOVA results of the corrugated paperboards.

Flute Type	Mean ECT Values (KN/m)		
	KS M 7063-1	TAPPI T 838	FEFCO No.8
A/F	5.69 (±0.76) A	6.29 (±0.79) A	4.04 (±0.85) B
B/F	5.10 (±0.80) A	5.90 (±0.74) A	4.47 (±0.88) B
AB/F	10.01 (±0.77) A	10.22 (±0.81) A	7.36 (±0.89) B
BB/F	9.42 (±0.79) A	11.00 (±0.78) A	7.66 (±0.90) B

Notes: All data represent the mean of five determinations. Values in parentheses are standard deviation values. The uppercase letters indicate the statistical difference in rows (significant level at 5%).

Though the magnitude of the experimental ECT values was different from the magnitude of the values produced by the FEA, there were similar trends depending on the standards and flute type. The main cause of the difference between the magnitude of the experimental ECT and FEA ECT values have been that the connection between the liner and flute was treated as a shared node instead of the actual condition of the connection using an adhesive. It was similar to the results of FEA ECT analysis, which differed by up to 45% from the results of the experiment of corrugated paper presented in the previous study [41]. In this study, simulations were conducted under the assumption that the liner and flute are fully bonding, and the theoretical interpretation of the adhesion properties is necessary, considering that the property of the adhesive is one of the important factors determining the strength of the corrugated paperboard during the adhesion process between the liner and flute of corrugated paperboard.

This difference also affected the failure mode difference between them. In the FEA, the failure mode was the localized buckling of the liner and the delamination between the liner and the flutes. However, in the experiment, delamination between the liner and flutes (mainly for KS M 7063-1 method A and TAPPI T 838) or edge crushing (mainly for FEFCO No.8) caused local buckling of the liner.

4. Conclusions

There is a growing concern regarding environmentally friendly packaging materials that can be returnable, and reusable due to environmental issues such as global warming and desertification. In this study, edgewise compression behaviors by different standards and flute types of corrugated paperboard were investigated using FEA and experimental analysis to replace the experimental methods with a faster FEA to determine the edgewise compression test value of the corrugated paperboard.

The summary of this study is listed below:

1. According to the FEA results, AB/F and A/F had greater ECT values than BB/F and B/F, respectively, for KS M 7063-1 method A. However, FEFCO No.8 had an opposite trend with the KS M 7063-1 method A. For TAPPI T 838, there was a mixed trend compared to the other standards. The experimental results also showed a similar trend for the different flutes as the FEA. The trend change between the A/F and B/F or AB/F and BB/F observed for the FEFCO No. 8 samples was the consequence of the relatively low height compared to the width and small slenderness ratio of the FEFCO No.8 test specimen, leading to the small effect of corrugated paperboard thickness on the edgewise compression behavior.

2. The FEA results showed that A/F, B/F, AB/F, and BB/F for FEFCO No.8 had 38% less, 16% less, 45% less, and 39% less ECT values than those values for KS M 7063-1 method A and TAPPI T 838. Meanwhile, the experimental results also showed that the ECT results of FEFCO No.8 were less than those of KS M 7063-1 method A and TAPPI T 838: 33% less (A/F), 19% less (B/F), 27% less (AB/F), and 25% less (BB/F). Though the experimental ECT values were different from the FEA ECT values, there were similar trends of ECT values depending on the standards and flute types. The main cause of the difference between the experimental ECT and FEA ECT values was that the connection between the liner and flute was treated as a shared node instead of the actual condition of the connection using an adhesive.

3. For the KS M 7063-1 method A and the TAPPI T 838, there was a local buckling of liners around the neck-down section, and the maximum stress generated at the edge of the neck-down section. For FEFCO No.8, however, the local buckling area of the liner was wide due to the uniformly distributed stress over the test specimen surface. Through experimental observation, it was observed that the delamination between the liner and the corrugating medium around the neck-down led to the total destruction of the test specimens for the KS M 7063-1 method A and TAPPI T 838, while it resulted in crushing and delamination at the top and bottom edge of the test specimen for FEFCO No.8.

4. Although the FE-based computer simulation technique overpredicted the ECT values of corrugated paperboard, it still can be a useful tool that can replace the ECT of corrugated paperboard if the material properties of the corrugated board components and the FE modeling methods are further investigated.

Appendix A

Appendix A.1. Generalized Equation for the Moment of Inertia of the Area of n-Layered Corrugated Paperboard

To represent the moment of inertia of the area for n-layered corrugated paperboard (the number of liner: n), it was expected to be useful to analyze surface properties of various corrugated paperboards and multi-layered corrugated structures.

This study developed a generalized equation for the moment of inertia of the area of the n-layered corrugated paperboard further investigating the moment of inertia of area analysis methods for various corrugated paperboards used in Lee and Park [42].
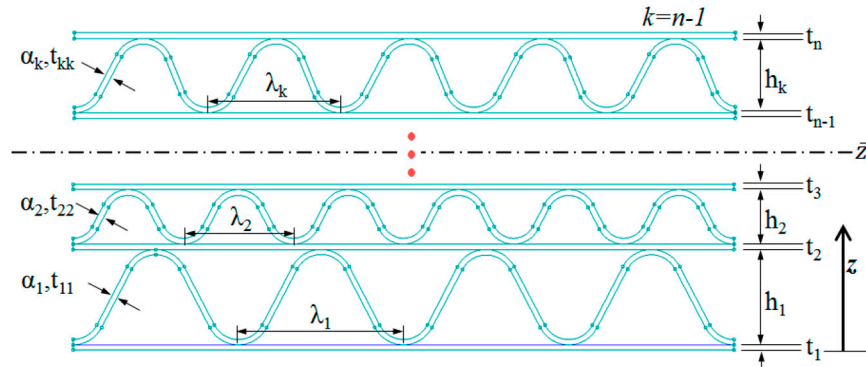

Figure A1. The CD cross-section of the n-layered corrugated board.

A generalized equation for the moment of inertia of the area of the n-layered corrugated paperboard could be developed with an assumption that the corrugated paperboard components consisted of the same materials (where the width of the n-layered corrugated paperboard $= \omega$, the thickness of the nth liner $= t_n$, the thickness of the kth corrugating medium $= t_{kk}$, height of the kth flute $= h_k$, and the take-up factor of the kth flute $= \alpha_k$).

- The neutral axis of CD cross-section of the n-layered corrugated paperboard:

$$\bar{z} = \frac{1}{A} \int_A z\, dA =$$
$$\frac{\sum_{n=1}^{n} t_n \left(\sum_{n=1}^{n-1} t_n + \frac{1}{2} t_n + \sum_{k=1}^{n-1} h_k \right) + \sum_{k=1}^{n-1} t_{kk} \alpha_k \left(\sum_{n=1}^{n-1} t_n + \sum_{k=1}^{n-2} h_k + \frac{1}{2} h_k \right)}{\sum_{n=1}^{n} t_n + \sum_{k=1}^{n-1} t_{kk} \alpha_k} \tag{A1}$$

- Moment of inertia of the area for the neutral axis of CD cross-section of the n-layered corrugated paperboard:

$$I_{\overline{xx}} = \sum_{n=1}^{n} \frac{\omega t_n^3}{12} + \sum_{n=1}^{n} \left(\bar{z} - \sum_{n=1}^{n-1} t_n - \frac{1}{2} t_n - \sum_{k=1}^{n-1} h_k \right)^2 \omega t_n + \sum_{k=1}^{n-1} (I_{\overline{xx}})_k + $$
$$\sum_{k=1}^{n-1} \left(\bar{y} - \sum_{n=1}^{n-1} t_n - \sum_{k=1}^{n-2} h_k - \frac{1}{2} h_{k-1} \right)^2 \omega t_{kk} \alpha_k \tag{A2}$$

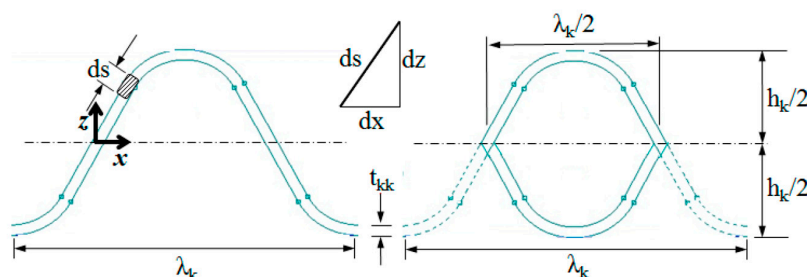- Moment of inertia of the area for the neutral axis of the CD cross-section of flute:

Figure A2. CD cross-section of flute.

for small area segment of flute, $dA \cong t_{kk}ds$; for small length segment of flute, $ds = \sqrt{1 + \left(\frac{dz}{dx}\right)^2} dx$.

If the shape of the flute is considered as a sinusoidal function, $z = \frac{h_k}{2} \sin \frac{2\pi x}{\lambda_k} \rightarrow \frac{dz}{dx} = \frac{\pi h_k}{\lambda_k} \cos \frac{2\pi x}{\lambda_k}$; therefore, the moment of inertia of the area of the neutral axis of the flute can be expressed in Equation (A3) or (A4):

$$(I_{\overline{xx}})_k = \int y^2 dA = \frac{4\omega}{\lambda_k}\left(\int_o^{\frac{\lambda_k}{4}} \frac{t_{kk}h_k^2}{4} \sin^2 \frac{2\pi x}{\lambda_k} \times \sqrt{1 + \frac{\pi^2 h_k^2}{\lambda_k^2} \cos^2 \frac{2\pi x}{\lambda_k}}\, dx\right) \tag{A3}$$

$$(I_{\overline{xx}})_k = \frac{\omega}{\lambda_k} \times \frac{\pi}{4}\left\{\left(\frac{h_k}{2}\right)^3\left(\frac{\lambda_k}{2}\right) - \left(\frac{h_k}{2} - t_{kk}\right)^3\left(\frac{\lambda_k}{2} - 2t_{kk}\right)\right\} \tag{A4}$$

Appendix A.2. Calculating the Moment of Inertia of the Area of Corrugated Boards Used in This Study

- SW corrugated board (A/F, B/F): $n = 2$, from Equations (A1), (A2), and (A4):

$$\overline{z} = \frac{\frac{1}{2}t_1^2 + t_2\left(t_1 + \frac{1}{2}t_2 + h_1\right) + t_{11}\alpha_1\left(t_1 + \frac{1}{2}h_1\right)}{t_1 + t_2 + t_{11}\alpha_1} \tag{A5}$$

$$I_{\overline{xx}} = \frac{\omega t_1^3}{12} + \frac{\omega t_2^3}{12} + \left(\overline{z} - \frac{t_1}{2}\right)^2 \omega t_1 + \left(\overline{\overline{z}} - \frac{t_2}{2}\right)^2 \omega t_2 + (I_{\overline{xx}})_1 + \left(\overline{\overline{z}} - t_2 - \frac{h_1}{2}\right)^2 \omega t_{11}\alpha_1 \tag{A6}$$

where, $\overline{\overline{z}} = (t_1 + t_2 + h_1) - \overline{z}$

$$(I_{\overline{xx}})_1 = \frac{\omega}{\lambda_1} \times \frac{\pi}{4}\left\{\left(\frac{h_1}{2}\right)^3\left(\frac{\lambda_1}{2}\right) - \left(\frac{h_1}{2} - t_{11}\right)^3\left(\frac{\lambda_1}{2} - 2t_{11}\right)\right\}$$

- DW corrugated board (AB/F, BB/F): $n = 3$, from Equations (A1), (A2), and (A4):

$$\overline{z} = \frac{\frac{1}{2}t_1^2 + t_2\left(t_1 + \frac{1}{2}t_2 + h_1\right) + t_3\left(t_1 + t_2 + \frac{1}{2}t_3 + h_1 + h_2\right) + t_{11}\alpha_1\left(t_1 + \frac{1}{2}h_1\right) + t_{22}\alpha_2\left(t_1 + t_2 + h_1 + \frac{1}{2}h_2\right)}{t_1 + t_2 + t_3 + t_{11}\alpha_1 + t_{22}\alpha_2} \tag{A7}$$

$$\begin{aligned}
I_{\overline{xx}} = &\frac{\omega t_1^3}{12} + \frac{\omega t_2^3}{12} + \frac{\omega t_3^3}{12} + \left(\overline{z} - \frac{t_1}{2}\right)^2 \omega t_1 + \left(t_1 + h_1 + \frac{t_2}{2} - \overline{y}\right)^2 \omega t_2 + \left(\overline{\overline{z}} - \frac{t_3}{2}\right)^2 \omega t_3 + (I_{\overline{xx}})_1 \\
&+ \left(\overline{z} - t_1 - \frac{h_1}{2}\right)^2 \omega t_{11}\alpha_1 + (I_{\overline{xx}})_2 + \left(\overline{\overline{z}} - t_3 - \frac{h_2}{2}\right)^2 \omega t_{22}\alpha_2
\end{aligned} \tag{A8}$$

where, $\overline{\overline{z}} = (t_1 + t_2 + t_3 + h_1 + h_2) - \overline{z}$

$$(I_{\overline{xx}})_2 = \frac{\omega}{\lambda_2} \times \frac{\pi}{4}\left\{\left(\frac{h_2}{2}\right)^3\left(\frac{\lambda_2}{2}\right) - \left(\frac{h_2}{2} - t_{22}\right)^3\left(\frac{\lambda_2}{2} - 2t_{22}\right)\right\}$$

Table A1. The calculation results of moment of inertia of area for each of flute type.

Flutes	Specifications	$\hat{z}$ (mm)	$I_{\overline{xx}}$ (mm^4)		
			Ω = 25 mm	Ω = 50 mm	Ω = 100 mm
A/F	$t_1 = t_2 = 0.20$, $t_{11} = 0.22$, $\lambda_1 = 9$ mm, $h_1 = 4.90$ m, $\alpha_1 = 1.560$	2.65	111.18	222.37	444.74
B/F	$t_1 = t_2 = 0.20$, $t_{11} = 0.22$, $\lambda_1 = 6$ mm, $h_1 = 2.65$ m, $\alpha_1 = 1.424$	1.52	31.87	63.73	127.47
AB/F	$t_1 = t_3 = 0.20$, $t_2 = 0.22$, $t_{11} = t_{22} = 0.22$, $\lambda_1 = 9$, $\lambda_2 = 6$ mm, $h_1 = 4.90$, $h_2 = 2.65$ m, $\alpha_1 = 1.560$, $\alpha_2 = 1.424$	4.52	286.39	572.79	1145.58
BB/F	$t_1 = t_3 = 0.20$, $t_2 = 0.22$, $t_{11} = t_{22} = 0.22$, $\lambda_1 = \lambda_2 = 6$ mm, $h_1 = h_2 = 2.65$ m, $\alpha_1 = \alpha_2 = 1.424$	2.96	137.16	274.33	548.65

Appendix A.3. Calculating the Slenderness Ratio of the Test Specimen for Each Standard

It was assumed that the KS M 7063-1 method A [13] was column-with-both-ends-built-in type, and TAPPI T 838 [14] and the FEFCO No.8 [15] were column-with-pinned-ends type in order to calculate the test specimen's slenderness ratios for each of standards [34].

$$\gamma = \frac{L_e}{k} \tag{A9}$$

$$k = \sqrt{\frac{I_{\overline{xx}}}{A}} \tag{A10}$$

where γ is the slenderness ratio, L_e is the effective buckling length (mm), k is the minimum radius of gyration (mm), $I_{\overline{xx}}$ is the moment of inertia of area (mm^4) for neutral axis, and A is the cross-section area (mm^2), respectively.

Table A2. The calculation results of the slenderness ratio for each flute type and standard.

Kinds		A (mm^2)	$I_{\overline{xx}}$ (mm^4)	K (mm)	L_e (mm) [1]	γ
KS M 7063-1 method A	A/F	37.16	222.37	2.45	30	12.24
	B/F	35.66	63.73	1.34	30	22.39
	AB/F	63.82	572.79	2.99	30	10.03
	BB/F	62.33	274.33	2.10	30	14.28
TAPPI T 838	A/F	18.58	111.18	2.45	50	20.41
	B/F	17.83	31.87	1.34	50	37.31
	AB/F	31.91	286.39	2.99	50	16.72
	BB/F	31.16	137.16	2.10	50	23.81
FEFCO No.8	A/F	74,32	444.74	2.45	25	10.20
	B/F	71.32	127.47	1.34	25	18.66
	AB/F	127.64	1145.58	2.99	25	8.36
	BB/F	124.66	548.65	2.10	25	11.90

Note: [1] $L_e = L/2$ for the column-with-both-ends-built-in type, and $L_e = L$ for the column-with-pinned-ends type [34].

References

1. Gilchrist, A.C.; Suhling, J.C.; Urbanik, T.J. Nonlinear finite element modeling of corrugated board. *Mech. Cellul. Mater.* **1999**, *85*, 101–106.
2. Haj-Ali, R.J.; Choi, B.S.; Wei, R. Refined nonlinear finite element models for corrugated fiberboards. *Compos. Struct.* **2009**, *87*, 321–333. [CrossRef]
3. Rahman, A.A.; Abubakr, S. A finite element investigation of the role of adhesive in the buckling failure of corrugated fiberboard. *Wood Fiber Sci.* **2004**, *36*, 260–268.
4. Baum, G.A.; Brennan, D.C.; Habeger, C.C. Orthotropic elastic constants of paper. *Tappi* **1981**, *64*, 97–101.

5.	Jiménez-Caballero, M.A.; Conde, I.; Garcia, B. Design of different types of corrugated board packages using finite element tools. In Proceedings of the SIMULIA Customer Conference, London, UK, 18–21 May 2009.

6.	Lorentzen & Wettre. *Lorentzen & Wettre Handbook*; Pulp and Paper Testing; Lorentzen & Wettre: Kista, Sweden, 2013.

7.	Armentani, E.; Caputo, F.; Esposito, R. FE analyses of stability of single and double corrugated boards. In Proceedings of the 4th International Conference on Axiomatic Design, Firenze, Italy, 13–16 June 2006; pp. 13–16.

8.	Maltenfort, G.G. *Performance and Evaluation of Shipping Containers*; Jelmar Publishing, Co.: New York, NY, USA, 1989; p. 475.

9.	McKee, R.C.; Gander, J.W.; Wachuta, J.R. Compression strength formula for corrugated boxes. *Paperboard Pack* **1963**, *48*, 149–159.

10.	Park, J.M.; Kim, G.S.; Kwon, S.H. Finite element analysis of corrugated board under bending stress. *J. Fac. Agric. Kyushu Univ.* **2012**, *57*, 181–188.

11.	Popil, R.E. Overview of recent studies at IPST on corrugated board edge compression strength: Testing methods and effects of interflute buckling. *BioResources* **2012**, *7*, 2553–2581. [CrossRef]

12.	TAPPI T 839 om-12. *Edge Compression Test for Strength of Corrugated Fiberboard Using the Clamp Method (Short Column Test)*; TAPPI: Peachtree Corners, GA, USA, 2009.

13.	Korean Standard Association (KSA). *Corrugated Fiberboard-Determination of Edgewise Crush Resistance*; KS M 7063; KSA: Seoul, Korea, 2015.

14.	TAPPI T 838 cm-12. *Edge Crush Test Using Neckdown*; TAPPI: Peachtree Corners, GA, USA, 2009.

15.	FEFCO NO.8. *Edgewise Crush Resistance of Corrugated Fiberboard*; FEFCO: Brussel, Belgium, 1997.

16.	ISO 3037: 2013. Corrugated Fibreboard—Determination of Edgewise Crush Resistance (Unwaxed Edge Method). Available online: https://www.iso.org/obp/ui/#iso:std:iso:3037:ed-5:v1:en (accessed on 3 September 2020).

17.	Korean Standard Association (KSA). *Corrugated Fiberboard—Determination of Edgewise Crush Resistance (Unwaxed Edge Method)*; KS M ISO 3037; KSA: Seoul, Korea, 2014.

18.	TAPPI T 811 om-11. *Edgewise Compressive Strength of Corrugated Fiberboard (Short Column Test)*; TAPPI: Peachtree Corners, GA, USA, 2009.

19.	ISO 13821:2002. *Corrugated Fibreboard—Determination of Edgewise Crush Resistance—Waxed Edge Method*; American National Standards Institute (ANSI): New York, NY, USA, 2007.

20.	Korean Standard Association (KSA). *Corrugated Fiberboard—Determination of Edgewise Crush Resistance (Waxed Edge Method)*; KS M ISO 13821; KSA: Seoul, Korea, 2014.

21.	Markström, H. *Testing Methods and Instruments for Corrugated Board*; Lorentzen & Wettre: Kista, Sweden, 1999; p. 104.

22.	Jiménez, M.A.; Liarte, E. Simulation of the edge crush test of corrugated paperboard using ABAQUS. In Proceedings of the ABAQUS World Users Conference 2003, Munich, Germany, 4–6 June 2003.

23.	Biancolini, M.E. Evaluation of equivalent stiffness properties of corrugated board. *Compos. Struct.* **2005**, *69*, 322–328. [CrossRef]

24.	Aboura, Z.; Talbi, N.; Allaoui, S.; Benzeggagh, M.L. Elastic behavior of corrugated cardboard—Experiments and modelling. *Compos. Struct.* **2004**, *63*, 53–62. [CrossRef]

25.	Hallbäck, N.; Korin, C.; Barbier, C. Finite element analysis of hot melt adhesive joints in carton board. *Packag. Technol. Sci.* **2014**, *27*, 701–712. [CrossRef]

26.	Han, J.G.; Park, J.M. Finite element analysis of vent/hand hole designs for corrugated fiberboard boxes. *Packag. Technol. Sci.* **2007**, *20*, 39–47. [CrossRef]

27.	Urbanik, T.J.; Saliklis, E.P. Finite element corroboration of buckling phenomena observed in corrugated boxes. *Wood Fiber Sci.* **2003**, *35*, 322–333.

28.	Nordstrand, T.M. Parametric study of the post-buckling strength of structural core sandwich panels. *Compos. Struct.* **1995**, *30*, 441–451. [CrossRef]

29.	Gospodinov, D.; Stefanov, S.; Hadjiiski, V. Use of the finite element method in studying the influence of different layers on mechanical characteristics of corrugated paperboard. *Tech. Gaz.* **2011**, *18*, 357–361.

30.	Korea Corrugated Packaging Case Industry Association (KCCA). 2013 production status of corrugated package. *Corrugat. Packag. Logist.* **2014**, *114*, 50–54.

31.	D'auria, A.; Marchese, P. Influence of the cutting procedure of specimens on the ECT test on corrugated board. *Cartotec. Imball.* **1982**, *6*, 15.

32. Korean Standard Association (KSA). *Corrugated Fiberboards for Shipping Containers*; KS T 1034; KSA: Seoul, Korea, 2014.

33. ANSYS Inc. *ANSYS Design Xplorer 14.5, Workbench User Guide*; ANSYS Inc.: Canonsburg, PA, USA, 2014.

34. Pilkey, W.D. *Formulas for Stress, Strain and Structure Matrices*; John Wiley & Sons, Inc.: New York, NY, USA, 1994; p. 1536.

35. ISO. *Paper and Board-Determination of Tensile Properties-Part 2: Constant Rate of Elongation Method (20 mm/min)*; ISO 1924-2:2008; British Standard Institute (BSI) and International Electrotechnical Commission (IEC): London, UK, 1995.

36. Persson, K. *Material Model for Paper: Experimental and Theoretical Aspects*; Diploma Report; Lund University: Lund, Sweden, 1991.

37. Mann, R.W.; Baum, G.A.; Habeger, C.C. Determination of all nine orthotropic elastic constants for machine-made paper. *Tappi* **1980**, *63*, 163–166.

38. International Organization for Standardization (ISO). *Paper and Board—Determination of the Static and Kinetic Coefficients of Friction—Horizontal Plane Method*; ISO 15359; ISO: Geneva, Switzerland, 1999.

39. Park, J.M.; Kim, J.S.; Park, J.H. Computer simulation and modeling of optimum clamping pressure in carton clamp handling for heavy corrugated package. *Mech. Ind.* **2020**, under publication.

40. R Core Team. *R Core Team: A Language and Environment for Statistical Computing*; R Foundation for Statistical Computing: Vienna, Austria, 2013. Available online: http://www.R-project.org/ (accessed on 28 June 2016).

41. Gudavičius, D. Finite Element Analysis of e-Commerce Corrugated Board Cushioning. Master's Thesis, KTH, Stockholm, Sweden, 2018.

42. Lee, M.H.; Park, J.M. Flexural stiffness of selected corrugated structures. *Packag. Technol. Sci.* **2004**, *17*, 275–286. [CrossRef]